

Variability of Antarctic Bottom Water at 24.5°N in the Atlantic

E. Frajka-Williams,¹ S. A. Cunningham,¹ H. Bryden,^{1,2} and B. A. King¹

Received 28 March 2011; revised 1 September 2011; accepted 6 September 2011; published 17 November 2011.

[1] A recent hydrographic section at 24.5°N in the Atlantic and 6 months of observations from a moored array show that Antarctic Bottom Water (AABW), the densest and deepest water mass in the world oceans, has been warming. While Johnson et al. (2008) showed that northward AABW transport at 24.5°N has been declining from 1981 to 2004, suggesting that the lower cell of the overturning circulation could halt in the near future, estimates from the latest hydrographic section in 2010 indicate a partial recovery of northward AABW transport. From 6 months of temperature and salinity observations at a deep moored array at 24–26°N, we find that short-term variability between April and November 2009 is of the same magnitude as the changes observed from hydrographic sections between 1981 and 2004. These observations highlight the possibility that transport changes estimated from hydrographic sections may be aliased by short-term variability. The observed AABW transport variability affects present estimates of the upper meridional overturning circulation by ± 0.4 Sv ($1 \text{ Sv} = 10^6 \text{ m}^3 \text{ s}^{-1}$).

Citation: Frajka-Williams, E., S. A. Cunningham, H. Bryden, and B. A. King (2011), Variability of Antarctic Bottom Water at 24.5°N in the Atlantic, *J. Geophys. Res.*, 116, C11026, doi:10.1029/2011JC007168.

1. Introduction

[2] The ocean meridional overturning circulation (MOC) is responsible for a large fraction of the poleward heat transport in the ocean [Trenberth and Caron, 2001]. In the Atlantic it is characterized by northward flowing warm waters near the surface, concentrated in the Gulf Stream at 26°N, and southward flowing cold waters between roughly 1000 and 5000 m, called the North Atlantic Deep Water (NADW). The overturning strength, estimated using the techniques described by Cunningham et al. [2007], is 18.6 ± 4.7 Sv between April 2004 to March 2009, with a strong annual cycle and subseasonal variability. Below this overturning circulation lies a deeper overturning cell; this lower cell is comprised of northward flowing Antarctic Bottom Water (AABW) at the bottom of the Atlantic which returns with the southward limb of the upper cell in the NADW. In the global context, the lower cell is of the same strength (roughly 20 Sv) as the upper overturning cell, though it carries less heat and only 6 Sv are in the Atlantic [Orsi et al., 1999].

[3] Recent observations have shown a warming of AABW both globally [Purkey and Johnson, 2010] and in the South Atlantic [Johnson and Doney, 2006]. Along the pathway of AABW into the North Atlantic, progressive warming of AABW has been observed in the Vema Channel (at 31–28°S and 39–40°W [Zenk and Morozov, 2007]), though observations further north at the equator and 36°W showed no warming [Limeburner et al., 2005]. In the North Atlantic,

Johnson et al. [2008] used a number of hydrographic sections to infer warming of AABW in the past several decades. Using four hydrographic sections at 24°N they show relative to 1981, that the northward transport of AABW has been monotonically decreasing through 2004 (hydrographic stations included in Figure 1c, which shows two additional sections).

[4] From the same hydrographic sections, transports of the full MOC were also calculated and similarly showed a monotonic decrease in the overturning strength on the order of 30% [Bryden et al., 2005] suggesting a possible collapse of the MOC. However, estimates of overturning from a moored array by the joint Rapid Climate Change-Will the Atlantic Thermohaline Circulation Halt (RAPID-WATCH)/Meridional Overturning Circulation and Heatflux Array (MOCHA) project showed that the subannual variability of the MOC since 2004 encompassed the 30% reduction in strength [Cunningham et al., 2007] and the monthly timing of the hydrographic sections in 1981, 1992, 1998, and 2004 corresponded to the peak to trough of the annual cycle of transports [Kanzow et al., 2010].

[5] What is the variability of AABW transport? Could the trends inferred by Johnson et al. [2008] be similarly aliased by high frequency variability? To investigate these questions, deep moorings were deployed in the western basin of the North Atlantic as part of the larger RAPID-WATCH/MOCHA mooring array (mooring schematic in Figure 1a). For the MOC calculation in the array, geostrophic transport per unit depth is estimated across 26°N using the dynamic height profiles from a series of moorings at the western boundary (WB), eastern boundary (EB) and mid-Atlantic ridge (MAR) [Cunningham et al., 2007]. However, these moorings only extended down to 4820 dbar. Below 4820 dbar, a fixed profile of transport per unit depth is used to represent AABW transport, summing to roughly 2 Sv [Kanzow

¹National Oceanography Centre, Southampton, UK.

²School of Ocean and Earth Science, University of Southampton, Southampton, UK.

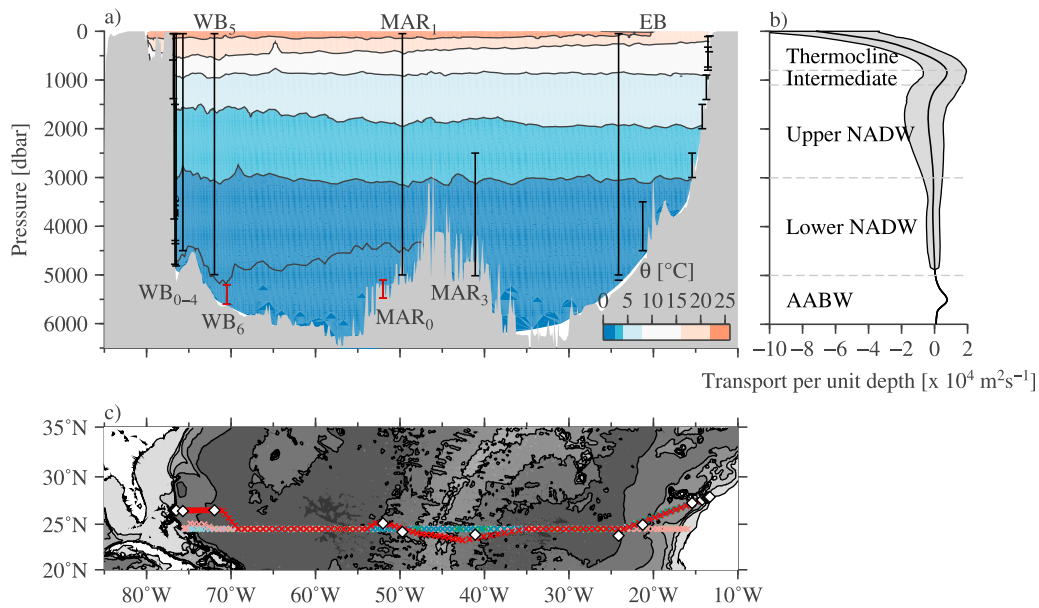


Figure 1. Array setup at 24–27°N in the Atlantic. (a) Potential temperature at 24–27°N in the Atlantic from the 2010 occupation of the line. Mooring locations from the RAPID-WATCH/MOCHA program are given by the vertical lines. The two red vertical lines highlight the deep moorings added for this study: in the abyss at 70.5°W (WB₆) and 52°W (MAR₀). (b) Transport per unit depth east of the Bahamas calculated from the moorings. The solid thick line is the mean while shading indicates the standard deviation between April 2004 and March 2009. The shear is divided into major water mass classes, including thermocline water, Antarctic Intermediate Water, North Atlantic Deep Water, and Antarctic Bottom Water. (c) Bathymetry around 20–35°N and station positions for six occupations of the hydrographic section, in 1957 (pale green), 1981 (light blue), 1992 (pink), 1998 (green), 2004 (dark blue), and 2010 (red). Mooring positions are given by white diamonds. Note, the 2004 and 2010 sections follow the same track except for near the mid-Atlantic ridge. The years 1957 and 1981 are across 24.5°N, as is 1992, with the exception of a deviation near the western boundary.

et al., 2010] (updated through April 2009 in Figure 1b). In 2009, two additional deep moorings were added below 4820 dbar to estimate the variability missed between 70°W and 52°W and deeper than 5100 dbar. In section 2, we describe the data and methodology. In section 3 we examine the short-term variability of transport and temperature fluctuations, from the mooring array. In section 4, we estimate transport and warming from the hydrographic sections, including a recent 2010 repeat of the 24°N hydrographic section [King, 2011], to put the mooring results in context and to revisit the calculation of Johnson *et al.* [2008]. We conclude with a discussion of the impacts of these findings on the MOC and our knowledge about the global overturning circulation.

2. Data and Methods

2.1. Moored Array

[6] Moorings used in this analysis are part of the RAPID-WATCH/MOCHA (hereafter referred to as RAPID) array at 24–28°N in the Atlantic (see Figures 1a and 1c for mooring positions). The array is used to estimate several components of the MOC including geostrophic transport between end point dynamic height moorings and absolute transport in the western boundary region from current meter arrays. When combined with the Gulf Stream transport through the Florida Straits and Ekman transports estimated from satellite wind

products, these produce a meridional overturning stream function at 26°N every 12 h (see Rayner *et al.* [2011] for a review).

[7] In this paper, we use the data from the two newly added deep moorings as well as two neighboring tall moorings, between 72°W and 49°W, between Florida and the mid-Atlantic ridge. The two deep moorings were WB₆ in the west at 26.49°N and 70.52°W and MAR₀ at the western flank of the mid-Atlantic ridge at 24.17°N and 52.01°W (Figure 1a). The tall moorings were instrumented throughout the water column: WB₅ at 26.50°N and 71.98°W, and MAR₁ at 24.16°N and 49.72°W (Figure 1a). WB₆ is in the abyssal plain, whereas MAR₀ is in a deep canyon of the mid-Atlantic ridge, chosen to have an open connection to the west at depth. WB₆ and MAR₀ were densely instrumented with five MicroCATs (Sea-Bird Electronics, Bellevue, Washington, USA), self-logging instruments which measure temperature, conductivity and pressure, from 5100 to 5600 dbar: WB₆ had four MicroCATs and MAR₀ had five providing a nominal vertical resolution of about 100 m. The high vertical resolution was motivated in part by the previous deep deployment which suffered high instrument loss rates due to flooding. The tall moorings WB₅ and MAR₁ had MicroCATs every 500 dbar near the seabed. MicroCATs measured temperature and conductivity every 30 min, and data were subsampled to 12 h and low-pass filtered with a 10-day filter. Bottom pressure recorders were also deployed, but as only

Table 1. Deep Transport Estimates From Hydrographic Sections Between Longitude Pairs^a

	70.5–46°W WB ₆ to 46°W (Sv)	70.5–49°W WB ₆ to MAR ₁ (Sv)	49–46°W MAR ₁ to 46°W (Sv)
1957	2.2	2.2	0.0
1981	3.7	4.0	−0.3
1992	3.2	3.2	0.0
1998	2.6	2.6	0.0
2004	2.6	2.6	0.0
2010	2.5	2.4	0.1
	2.8 ± 0.6	2.8 ± 0.7	0.0 ± 0.1

^aTransports are calculated as a zonal-integral of geostrophic shear referenced to 4100 dbar between the nearest stations to each mooring longitude. Unlike the transport estimates in Figure 9b which only considers transport of water colder than 1.8°C, these estimates are for total transport below 4100 dbar. Transports in this table are for comparison with the mooring data, which cannot be limited to water colder than 1.8°C.

one of the two bottom pressure recorders was successfully recovered, bottom pressure is not used in this study.

[8] MicroCAT temperature, conductivity, and pressure are calibrated using a combination of Sea-Bird laboratory calibrations and pre- and postdeployment calibration dips using the vessel-mounted Seabird conductivity-temperature-depth (CTD). The purpose of the dips is to remove any trends due to sensor drift. For pressure, the signal varied due to drift as well as blowdown by large currents. While typical pressure variations due to blowdown were 100–200 dbar at WB₅ near the surface, they were only 30 dbar below 4000 dbar. Pressure drifts were corrected using an exponential-linear fit to the entire record. On WB₆ and MAR₀, pressure drifts of the Paine pressure sensors were quite large, on the order of 20 dbar over the 1 year deployment, with some drifts toward increasing pressure while others drifted toward decreasing pressure. In addition, two MicroCATs that were deployed adjacent to each other on the rope (separated by less than 1 m vertically) returned initial pressure readings that were 26 dbar apart. In this instance, pressures were adjusted using the relative spacing between instruments and the bottom depth. For WB₆ and MAR₀, the applied corrections ranged from −6 to 26 dbar. For a typical salinity of 34.85 and temperature of 1.8°C at 5100 dbar, a ±5 dbar offset in pressure would result in ±0.0019 offset in salinities, and a ±0.0001 kg m^{−3} offset in density.

[9] We estimate AABW transport between 70.5°W (WB₆) and 49°W (MAR₁) and below 4100 dbar. Since WB₆ and MAR₀ only had instruments below 5000 dbar, the data from WB₅ and MAR₁ are used to extend the transport profiles between 4100 and 5100 dbar (WB) and 5300 dbar (MAR). At the western edge, in comparing temperature and salinity at 72°W and 70.5°W, we found that differences above 4700 dbar are very small (not shown), and so used data from WB₅ at 4620 and 4100 dbar. At the mid-Atlantic ridge, we used data from MAR₁ at 5160, 4640, and 4130 dbar. At the mid-Atlantic ridge, these estimates neglect transport in the bottom triangle (below 5300 dbar and between MAR₀ and MAR₁). To estimate this error, we calculated transport in the bottom triangles using hydrographic sections. Overall the transport neglected here was 0.0 ± 0.1 Sv (see Table 1). Temperature and salinity profiles at the west and mid-Atlantic ridge are linearly interpolated onto a regular 20 dbar grid before density is calculated. Geostrophic transports are

calculated between the two profiles, relative to 4100 dbar. This choice of level-of-no-motion will be justified below from hydrography. Below the deepest common level (5600 dbar), transport profiles are extrapolated to zero at 6300 dbar.

2.2. Hydrographic Sections

[10] Six hydrographic sections at 24°N in the Atlantic are used from 1957, 1981, 1992, 1998, 2004, and 2010. Table 2 contains details of the sections, and Figure 1c shows the tracks. Latitudes at the western and eastern boundaries varied between early and later sections, and the 2010 section followed the Kane Fracture Zone, the deepest path across the mid-Atlantic ridge in the area (see the non-zonal segment of the red transect between 40 and 55°W in Figure 1c). As technology has improved, longitudinal resolution has increased, the 1957 section occupied 38 stations, compared with the 2010 section that occupied 122 stations between 13° and 77°W. The 2010 section also recorded the deepest measurements along the transect, reaching 6851 dbar (see Figure 2 and Figure 3).

[11] In order to compare AABW volumes and properties between sections with variable resolution and maximum bottom depths, data are gridded onto a uniform longitude-depth grid. In particular, early sections were sparsely sampled in longitude so that the station separation in 1957 was 162 ± 48 km compared to 55 ± 23 km in 2010. Data from each section is linearly interpolated onto a fine longitudinal grid (1000 points between 77 and 13°W) and a 1 dbar pressure grid. The 2004 section was limited by instrumentation to a maximum bottom depth of 6000 dbar, even though the water depth was closer to 6400 dbar. The 2010 section, for which casts extended to within 10 m of the bottom, shows that profiles of temperature and salinity are well-mixed in the bottom 500 m in water depths greater than 4000 dbar (e.g., standard deviation of temperature less than 0.025°C and of salinity less than 0.003). For all stations with water depths greater than 4000 dbar, temperature and salinity profiles are extended to the bottom depth using the deepest measurements in the profile. Bottom depth is used at 24.5°N, rather than along the track lines, to reduce variations due to latitudinal changes between section occupations. Bottom depth is estimated from ETOPO bathymetry [U.S. Department of Commerce, 2006]. As an example of the effect of filling the profiles on volume estimates, in 2004, roughly 20% of the water colder than 1.8°C is from the filled bottom of the profiles.

[12] Transports at 24°N have been calculated with several combinations of geostrophic reference levels (as described by Lavin *et al.* [1998]) including 3200 dbar, 4000 dbar, a

Table 2. Hydrographic Sections, Number of Stations East of 77°W, and the Mean and Standard Deviation of Distance Between Stations

Year	Ship	Dates	Number of Stations	Spacing (km)
1957	RRS <i>Discovery II</i>	6–28 Oct	38	162 ± 48
1981	RV <i>Atlantis</i>	12 Aug–6 Sep	90	71 ± 31
1992	BIO <i>Hespérides</i>	20 Jul–16 Aug	101	61 ± 13
1998	RV <i>Ronald H. Brown</i>	23 Jan–24 Feb	121	55 ± 23
2004	RRS <i>Discovery</i>	4 Apr–10 May	113	59 ± 26
2010	RRS <i>Discovery</i>	5 Jan–19 Feb	122	55 ± 23

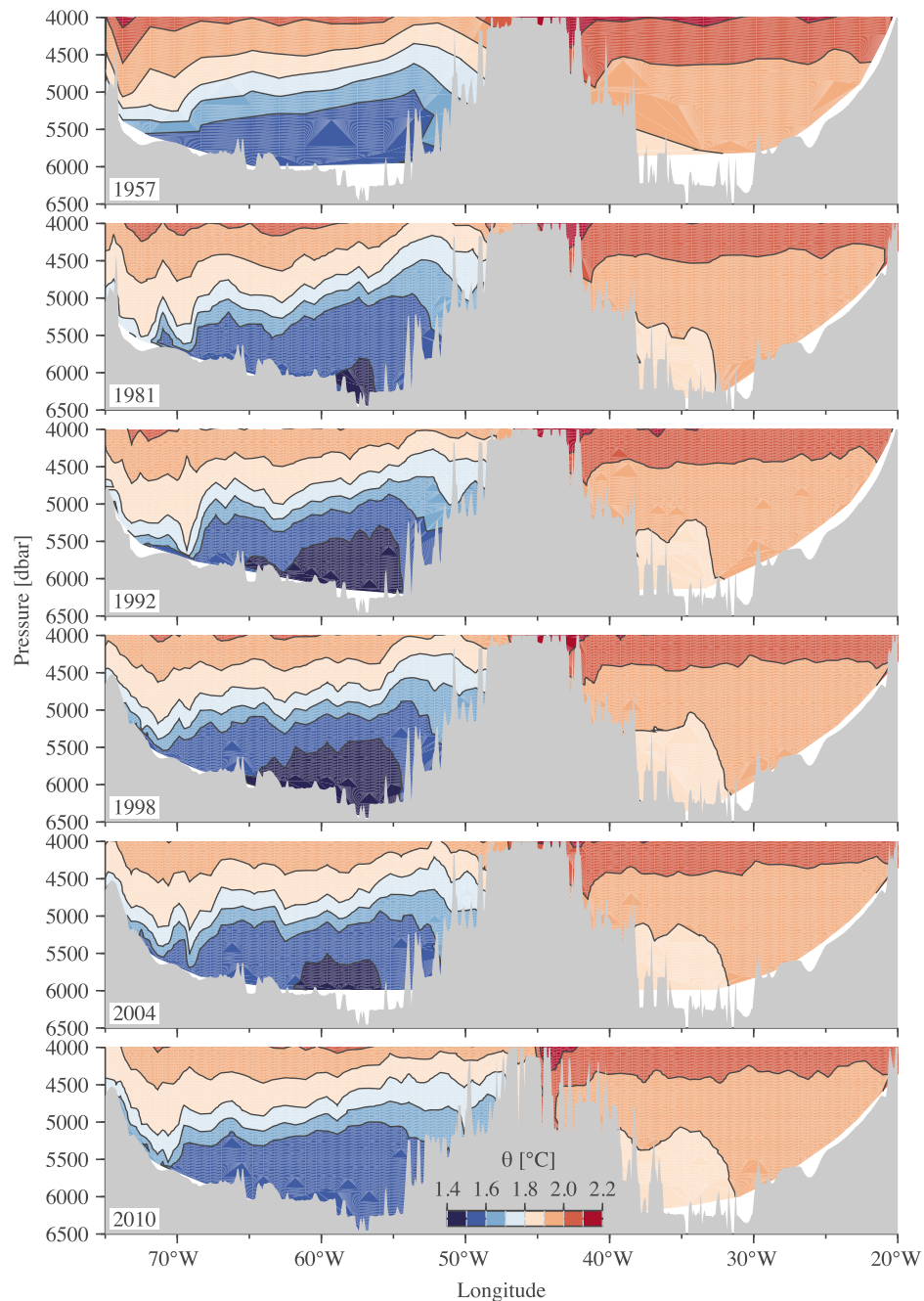


Figure 2. Deep potential temperature sections from the six hydrographic cruises at 24.5–26.5°N in the Atlantic. Contours of potential temperature are at 0.1°C intervals. Bathymetry is shaded and represents the bottom depth from ETOPO along each hydrographic section.

different reference level in the deep western boundary current region as the rest of the basin, and including a barotropic correction to ensure no net transport across the section. Here we calculate transport profiles from geostrophic meridional velocities using a 4100 dbar zero-velocity reference level for the section east of the deep western boundary current area. This level-of-no-motion minimizes net transport in the eastern basin below the mid-Atlantic ridge (using a ridge depth of 4000 dbar). For the six hydrographic sections, the net eastern basin transport (east of 46°W and below 4000 dbar) was 0.0 ± 0.3 Sv northward.

Recent evidence from the RAPID observations suggest that the barotropic velocities are largest in the western boundary region, not uniformly distributed across the entire basin width [Johns *et al.*, 2008; Bryden *et al.*, 2009]. We can still enforce a mass balance between the geostrophic transport estimates, Ekman, Gulf Stream and Bering Strait transports, but for our purposes, this would be confined to the region west of 70.5°W. Transport values for each year, with the 4100 dbar geostrophic reference level, are given in Table 3. A second set of transport calculations is done with a 3200 dbar reference level, as in the work of Johnson *et al.*

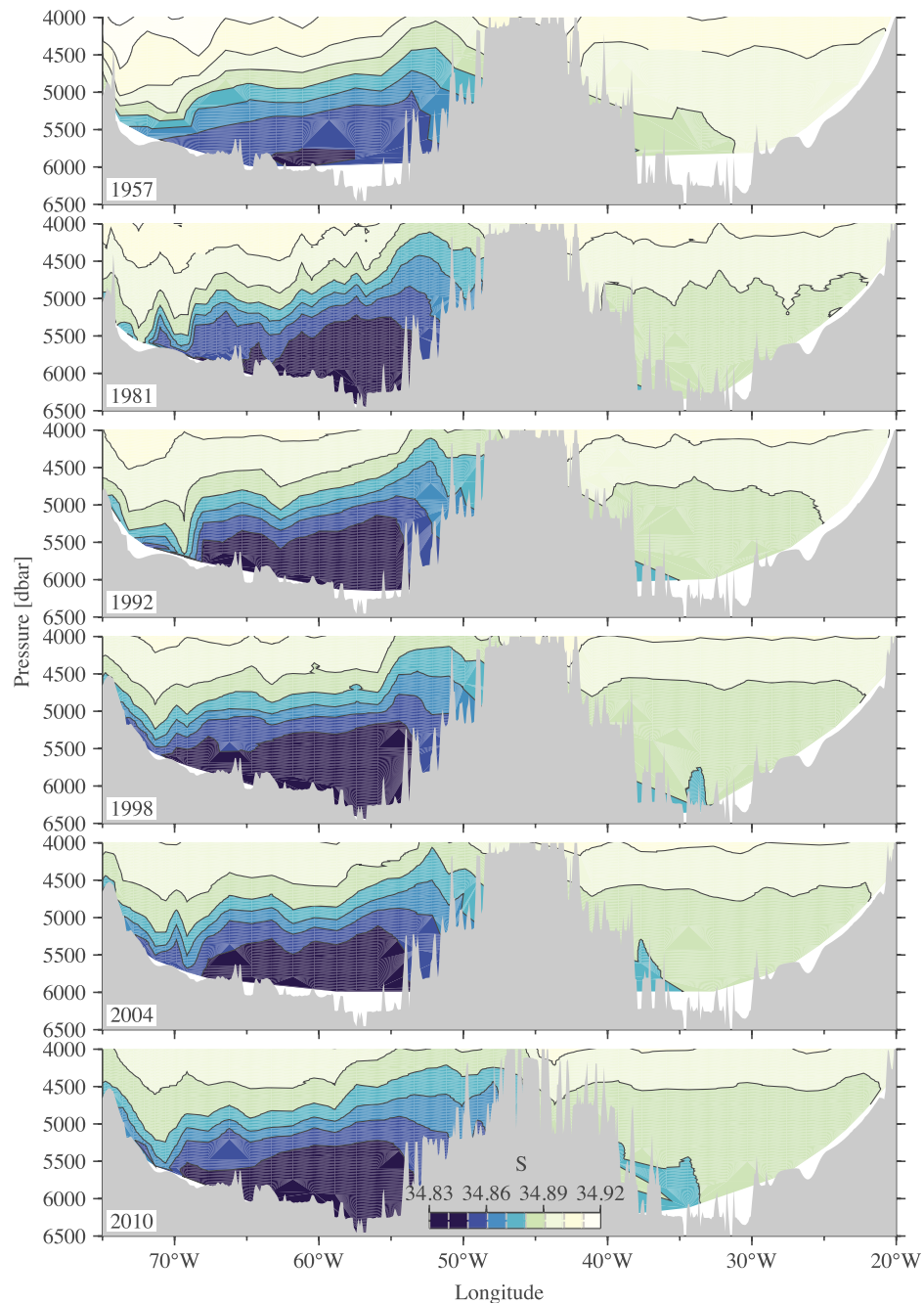


Figure 3. Deep salinity sections from the six hydrographic cruises at 24.5–26.5°N in the Atlantic. Contours of salinity are at 0.01 intervals. Bathymetry is shaded and represents the bottom depth from ETOPO along each hydrographic section.

[2008], with no barotropic velocity applied. In this instance as well, it would be possible to apply the barotropic compensation to the west of the AABW transport region.

3. Results: Moorings

3.1. AABW Property Variability

[13] Temperature variations are typically vertically coherent. In April and May 2009, a large warm anomaly was visible at both mooring sites at WB₆ and MAR₀ (Figure 4). In such

weak stratification, these small temperature changes represent large vertical displacements of isotherms (roughly 150–300 dbar, not shown). A large cooling signal was also observed in September across four of the five instruments on WB₆.

[14] These large warm fluctuations in WB₆ persisted for about three weeks (late April to mid-May) with a peak-to-peak temperature range of over 0.1°C at 5400 dbar (See Figure 4a). The reverse event in September 2009 was quite brief by comparison (17 September to 24 September). At

Table 3. Ekman, Florida Current, and Bering Strait Transports Used for Mass Balance in the Hydrographic Sections^a

	Ekman (Sv)	Florida Current (Sv)	Bering Strait (Sv)	Barotropic ^b (cm s ⁻¹)
1957	4.5	31.1	-0.8	0.0
1981	3.7	31.1	-0.8	-0.2
1992	4.6	30.3	-0.8	1.7
1998	5.2	34.0	-0.8	-0.4
2004	4.5	31.8	-0.8	0.2
2010	4.1	31.6	-0.8	-0.3

^aEkman and Florida Current transports for 2010 were the average values from 2008.

^bThe amount of barotropic velocity which was necessary to apply west of 70.5°W in order to achieve mass balance across the section.

MAR₀, similar warm fluctuations were seen, both in January 2009 and a larger one in May 2009. The May event appears to be bottom intensified with the sharpest changes at 5500 dbar (about 0.05°C in a couple days, 6 May to 8 May).

[15] The data also show a small, longer period warming trend in the deepest MicroCATs on MAR₀ of 0.03°C over the 360 day deployment, calculated as a linear fit to the data (See Figure 4b). Salinities increased by roughly 0.04 over the same period (not shown). While we cannot conclude from the warming at MAR₀ that the whole of AABW is warming, the deepest instruments on MAR₁ also showed a warming (on the order of 0.015°C). The warming at both locations may be due to a zonal repositioning of the sloping isotherms between MAR₀ and the ridge, but it is also consistent with a longer term warming trend.

[16] Comparing the data to the nearest hydrographic casts (Figure 5a), we see that the $\theta - S$ range at WB₆ lies most

closely along the 2010 profile and that the warm, salty fluctuations are along the $\theta - S$ curve rather than a shift in the $\theta - S$ relationship. Variance in temperature and salinity are plotted as ellipses along the major and minor axes of variability following *Emery and Thompson* [2004]. At MAR₀, the 1981 casts were colder and saltier than both the more recent casts and the mooring data, even including variability given by the standard deviations of temperature and salinity (Figure 5b). The long term warming from hydrography, both at WB₆ and MAR₀ is stronger than the short-term variability observed at the mooring sites.

3.2. AABW Transport Variability

[17] Overall, the range in transports over the 6-month period, below 4100 dbar, was 1 to 3 Sv, with a standard deviation of 0.4 Sv (Figure 6). Comparing this to the previous decades, the range is larger over the 6 month deployment than between the six hydrographic sections, where transport ranged from 2.2 to 3.7 Sv (Table 1) though the mean is smaller. Note that the AABW transport estimates from hydrography in Table 1 are calculated differently than in the later section on hydrography where only water colder than 1.8°C will be included. For comparison with the moorings, where the transport cannot be partitioned by temperature, the values in Table 1 include all water below 4100 dbar.

[18] Transport variability is dominated by changes at the deepest instruments on WB₅ in the western boundary. These transports have been estimated for the overlap period between WB₆ and MAR₀, from April to November 2009 using transport profiles which have been extrapolated to zero below 5600 dbar. There were several increases in

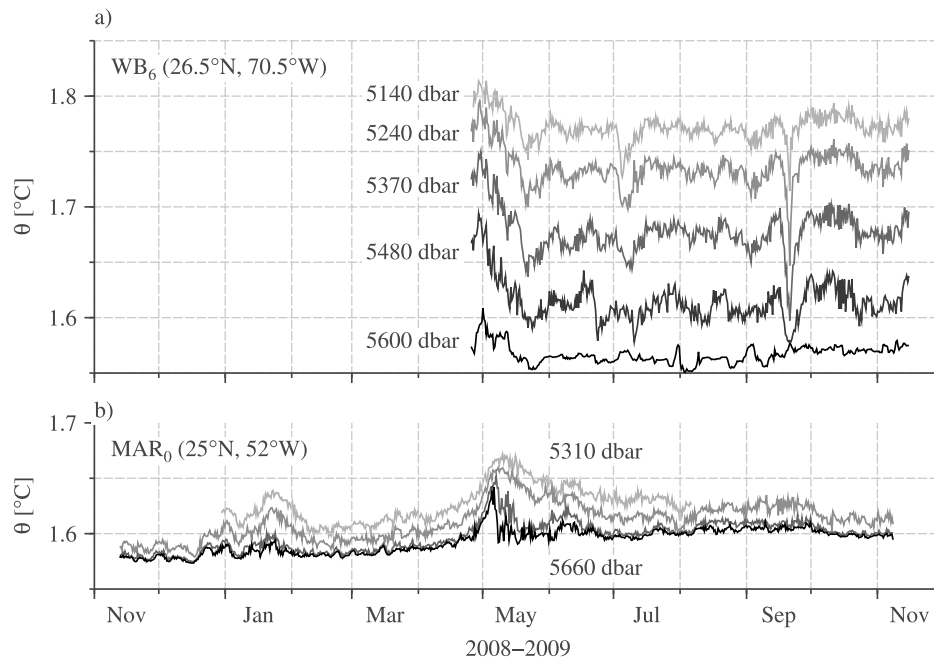


Figure 4. Potential temperature from (a) WB₆ and (b) MAR₀ from each moored MicroCAT. Pressure annotated are approximate averages for each record from WB₆ and the range for the four instruments on MAR₀ (5310, 4330, 5580, and 5660 dbar). Instruments were spaced at 100 dbar intervals. Data have been calibrated and subsampled to 12 hourly intervals.

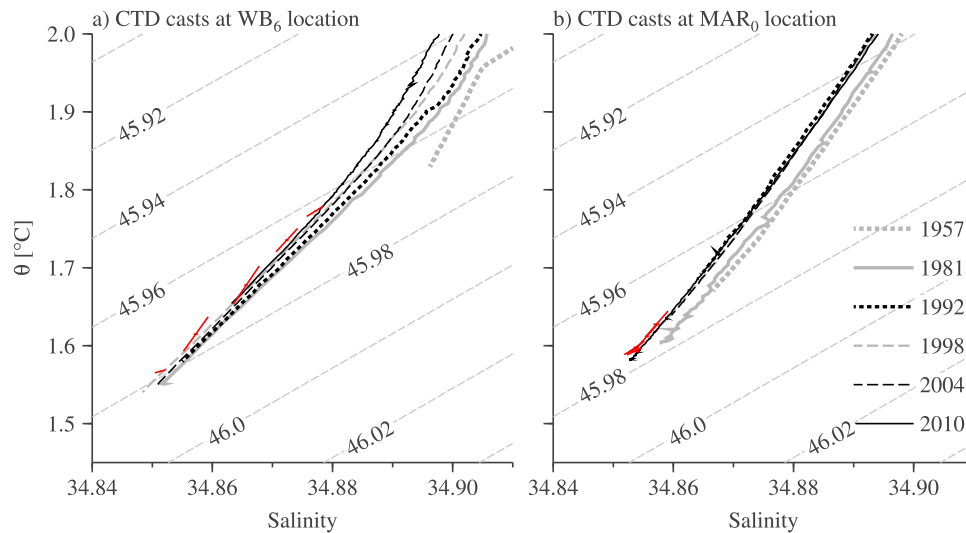


Figure 5. Temperature and salinity from the six hydrographic sections at the two deep mooring sites, (a) WB_6 and (b) MAR_0 . Temperatures and salinities from the mooring deployments are given by the red crosses, where the axes are standard deviations along the major and minor axes of variance ellipses. Potential density (σ_4) is contoured.

transport, which peaked at the beginning of May, mid-June, and the beginning of August, that corresponded to increases in temperature at WB_6 (Figure 4a). There was also a large increase in transport in the last month (November) resulting from a general warming in the upper layers near the bottom of WB_5 . The gradual warming at both MAR_0 and MAR_1 results in a slow decline of AABW transport (until the November reversal).

[19] Transport profiles between $70.5^\circ W$ and $49^\circ W$ are shown in Figure 7. Profiles have been averaged by month and the profiles calculated from the nearest hydrographic stations in 1981, 2009 (calibration casts), and 2010 are shown as well. The figure includes April through October, with November having been omitted as short (<2 weeks). The structure and magnitude of transport profiles in the seven month mooring period matches the previous estimates. However, the local bottom depth at WB_6 and MAR_0 is at 5600 dbar. Transport per unit depth estimates from hydrography (section 4.3) show that, for example, in 2010, 0.6 Sv or 20% of the AABW transport was located below

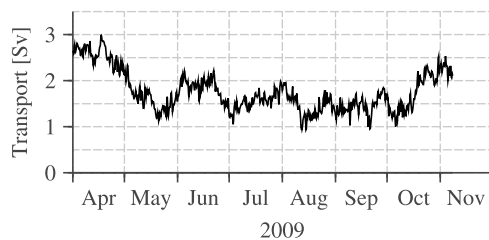


Figure 6. Net transport below 4100 dbar between 70.5 and $49^\circ W$ estimated from mooring data over the period where the WB_6 and MAR_0 deployments coincided. Below the deepest common level (5600 dbar), each transport profile has been extrapolated to zero at 6300 dbar.

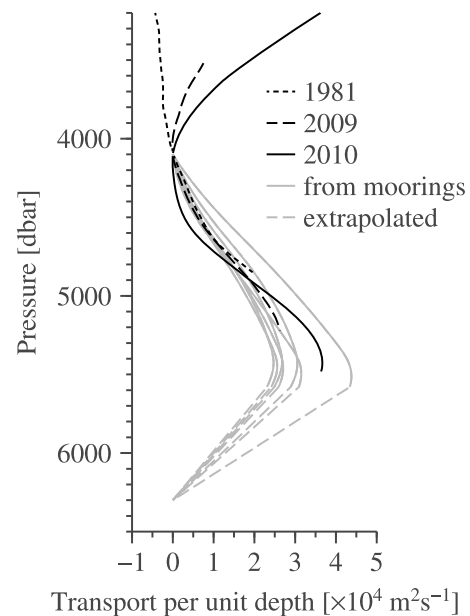


Figure 7. Transport profiles from moorings (gray) and hydrography (black) between 70.5 and $49^\circ W$, relative to a level-of-no-motion at 4100 dbar. Hydrographic data from 2009 is from CTD casts during the mooring deployment cruise. Estimates from hydrographic data use the shear between the stations nearest the mooring locations, so transport estimates are limited to the depth range above the deepest common level between the two stations. Mooring transport estimates are averaged by month (April–October, November having been omitted since the record is short). Dashed gray lines show transports linearly extrapolated to zero the 6300 dbar.

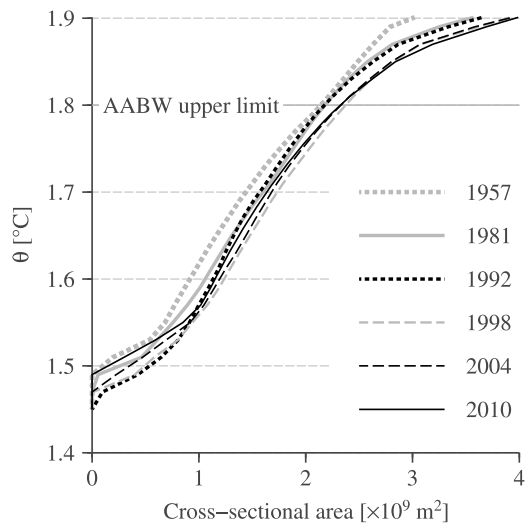


Figure 8. Cumulative volume of water colder than a given temperature estimated as a cross-sectional area across 24.5°N between 77°W and 20°W from hydrographic sections. Before estimating volume, station data were gridded onto a fine pressure-longitude grid and the bottom of each profile was filled by continuing the deepest measurement down to bathymetry estimates across 24.5°N . Using bathymetry at 24.5°N rather than at station positions reduces differences in volume estimates due to varying cruise track positions. Water colder than 1.8°C is called AABW.

5600 dbar. In addition, the transport between 49°W and 46°W is neglected. However, from the transport estimates between these two longitudes from hydrography (Table 1), we can see that this contribution is very small or nil.

4. Results: Hydrographic Sections

4.1. AABW Property Changes Across Decades

[20] The six hydrographic sections show similar overall structure and properties of AABW from 1957 to 2010 (See Figures 2 and 3). The water below 4500 dbar is cold ($\theta < 1.9^{\circ}\text{C}$) and relatively fresh ($S \sim 34.89$) compared with the overlying NADW ($\theta > 1.9^{\circ}\text{C}$ and $S > 34.899$). Comparing the sections, the contour choice highlights the change in the coldest water masses: in 1957, no water colder than 1.5°C was measured (Figure 2). The volume of water colder than 1.5°C increased from nothing in 1957 to its peak in 1992 before its near absence in 2010. This suggests that the volume of coldest AABW at 24.5°N has fluctuated.

[21] By comparing the cross-sectional area of water colder than a particular isotherm, we can compare variations in volume between years (Figure 8). The particular trends apparent are that below 1.54°C , 1992 had the largest volume (estimated from cross-sectional area) of water which decreased monotonically through the 1998, 2004, and 2010 sections. However, at warmer isotherms, e.g., 1.7°C , the pattern is not the same. The volume of water colder than 1.7°C was greatest in 1998, and somewhat less in subsequent sections. If we look at total AABW volume, defined as water colder than 1.8°C (following *Johnson et al.* [2008] and *Lavin et al.* [2003]), the most recent three sections, including 2010, had the largest volume of water. These

changes indicate that rather than an overall contraction of AABW volume at 24.5°N , the properties of AABW have shifted toward a slightly warmer mean temperature with a decrease in the volume of water colder than 1.5°C since 1992, but a larger overall volume of water colder than 1.8°C since 1998.

4.2. AABW Structure and Volume

[22] AABW, as delineated by the 1.8°C , has isotherms that slope up from 70°W to 55°W , then deepen toward the mid-Atlantic ridge (see Figure 9a). By the thermal wind relationship, the upwards slope to the east is indicative of northward flow below. West of 70°W , isotherms follow bathymetry. The slope of the isotherms has zonal structure that persists in all six sections. From 70°W to 66°W , the slope is steepest, indicative of faster northward flow. From 66°W to 61°W , isotherms are nearly level, before they shoal again from 61°W to 52°W . This temperature structure follows structure of the bathymetry north of 24°N where a submarine ridge divides the deep western basin into a small basin to the west and the larger basin to the east (see Figure 1). The pattern of slopes in isotherms suggest a northward flow at the mid-Atlantic ridge, southward recirculation around $66\text{--}61^{\circ}\text{W}$, and northward circulation between 70°W and 66°W .

[23] In addition, there appear to be small-scale, possibly eddy, features. In the 2004 section, there is a localized shoaling of isotherms at 70°W . Considering the slope of isotherms from the western endpoint of AABW to 46°W , the basin-wide slope is reduced for a western end point of 70°W , in an eddy and relatively enhanced for 70.5°W . Since eddy features are likely to be transient, and not necessarily representative of large-scale changes in AABW transport, we avoid integrating transports from an end point within an eddy and use a western integration limit of 70.5°W rather than 70°W .

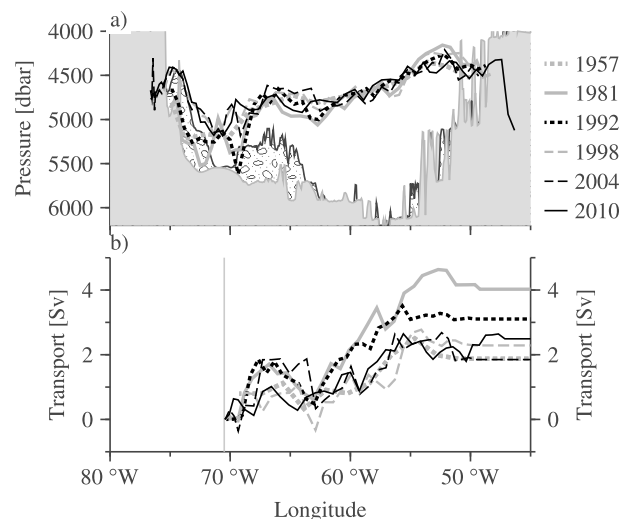


Figure 9. (a) Depth of the 1.8°C isotherm (in dbar) from the six hydrographic sections. The bathymetry at 24.5°N is shaded in light gray. The bathymetry at 27°N is shaded in the hachure pattern. Note the elevated bathymetry around $65\text{--}70^{\circ}\text{W}$. (b) Cumulative transport of AABW (water with $\theta < 1.8^{\circ}\text{C}$) from the hydrographic sections, integrated from zero at 70.5°W to the east.

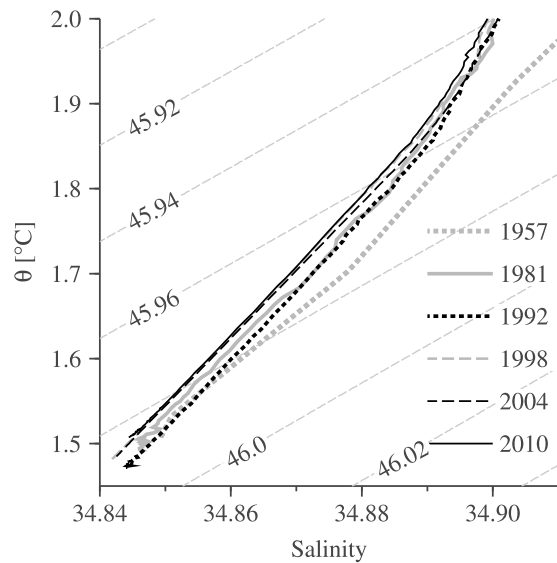


Figure 10. The $\theta - S$ plot from the coldest core of AABW for each hydrographic section. Contours are potential density referenced to 4000 dbar (σ_4).

[24] The core of AABW (as given by the coldest temperatures measured at 5990 dbar, the deepest measurements common to all six sections) also changes position from section to section. Most years, the core is between 58.8–57.8°W except in 1957 and 2010 when it moved west to around 61°W (not shown). The vertical structure of temperature and salinity at the core stations reveals a large volume of weakly stratified water below about 5200 dbar with a thermocline above. Temperatures in the most recent three sections warm more rapidly in the thermocline with distance from the bottom. Salinities shift more gradually between occupations, showing some variation in the most recent three sections. A small but progressively warming and salinification of the deep, weakly stratified layer is apparent from 1998 to 2010.

[25] The $\theta - S$ profiles from the core stations are shown in Figure 10. Very little variation is apparent in the most recent three sections except that the extreme of the coldest, freshest range is progressively disappearing. Again, the 2010 hydrographic section shows the absence of coldest, freshest water.

[26] The pattern of change between sections is shown in Figure 11. Note that the latitude of sections deviated at the western boundary and the mid-Atlantic ridge (Figure 1c); early sections were along a single latitude, 24.5°N while later sections connected with the Florida Straits in the west (26.5°N). Temperature comparisons in the western basin are only valid east of 68°W. Johnson *et al.* [2008] described a pattern of warming and cooling that indicated a decrease in the tilt of the isotherms between the 1981 to 2004 section (Figure 11a). This pattern was not continued in 2010. Instead, since 2004, the entire volume of AABW below 5500 dbar has warmed (below the average position of the 1.6°C isotherm, while above 4000 dbar or the 2.0°C, the water has warmed. Between 4000 and 5500 dbar, the region between 65 and 68°W and between 55 and 50°W has warmed and between the two has cooled. These changes will work to decrease the recirculation noted above, smoothing the isotherm depth in 2010 (as can be seen in Figure 9a). From 1981

to 2010, above the 2°C isotherm, the region east of 60°W has warmed, while west of 60°W has cooled. These changes will affect shear in the NADW layers, but due to our choice of reference level at 4100 dbar, will not project onto AABW transport estimates here. The total effect since 1981 has been a warming of the deepest layers of AABW (below 5500 dbar) and a cooling of the water below 4100 dbar.

4.3. AABW Transport Across Decades

[27] The relative strength of AABW transport from the six hydrographic sections is mostly insensitive to the choice of longitudinal limits or reference level. The zonally integrated transport of water colder than 1.8°C from 46°W to a variable western longitude limit, and relative to a reference level of 3200 or 4100 dbar is shown in Figures 12a and 12b, respectively. The x-axis represents the western limit of integration. From this we can see that for any western limit and either reference level, 1981 had the highest northward transport of AABW. Note that the values change slowly in most cases for a given year and have varying longitude limits. Two exceptions are the localized dips in transport for 1981 at 71°W and for 2004 at 70°W. These may be local transient eddies which deflect isotherms and would then not

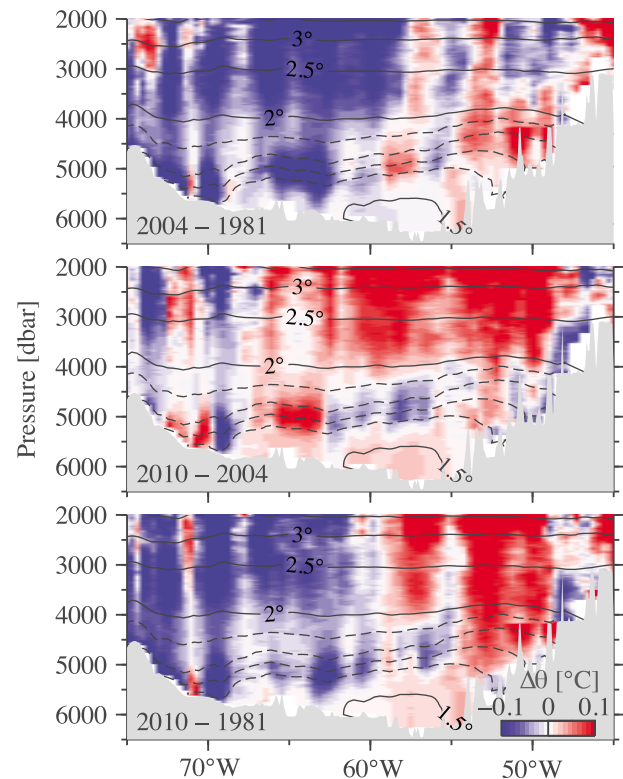


Figure 11. Temperature changes between (a) 1981 and 2004, (b) 2004 and 2010, and (c) 1981 and 2010, calculated as modern minus older. Red regions indicate warming while blue regions indicate cooling. Temperatures were first gridded for each hydrographic section data onto a fine pressure-longitude grid before differencing. Isotherms contoured are the mean isotherm depths (in dbar) from the sections 1981, 1992, 1998, 2004, and 2010 at 0.5° intervals in solid black, and between 1.5°C and 2.0°C at 0.1°C intervals in dashed black.

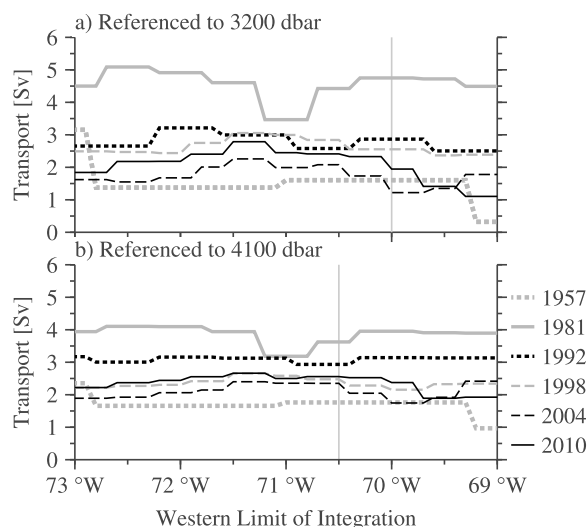


Figure 12. Effect of choice of reference level and longitude limits on AABW transport estimate. (a) The zonal integral of transport from 46°W to the western limit of integration (x-axis), referencing geostrophic velocity to 3200 dbar. The vertical line is the western limit used in the work of *Johnson et al.* [2008]. (b) The same as in Figure 12a except referencing geostrophic velocity to 4100 dbar. The vertical line is the western limit used here.

be representative of the overall transports. The range between 1981 and 2004 transports is larger when using a 3200 dbar reference level. Additionally, using the reference level of 3200 dbar, the magnitude of reduction in AABW transport from 1981 to 2004 was accentuated by the particular choice of western longitudinal limits from *Johnson et al.* [2008]. However, with few exceptions, the monotonic reducing trend in transports between 1981 and 2004 is apparent regardless of the choice of longitudinal limits or reference level.

[28] Similarly, for both reference levels and a range of longitudinal limits, the transport in 2010 of water colder than 1.8°C is similar to that observed in 1998, and about average for all the sections except for 1981. For our choice of a 4100 dbar reference level and a 70.5°W west limit, while total transport decreased monotonically from 1981 (3.7 Sv) to 2004 (2.4 Sv), there was a resurgence of AABW in 2010 (2.8 Sv), giving an overall mean value of 2.8 Sv for the six sections and standard deviation of 0.6 Sv.

5. Discussion

[29] From hydrographic sections between 1957 and 2010, and continuous mooring records in 2008–2009, we have estimated transport and property changes in AABW at 24.5°N in the Atlantic. The coldest core of AABW (found between 57°W and 61°W) has warmed since 1992; while the overall volume of AABW has not changed, the coldest vintages have disappeared. A similar warming trend was observed in the mooring records, consistent with the recent global warming of AABW estimated from hydrographic sections in the work of *Purkey and Johnson* [2010], in the South Atlantic [*Johnson and Doney*, 2006], and through the Vema channel [*Zenk and Morozov*, 2007].

[30] There are two main distinctions between our analysis of the mooring data and the hydrographic data. Moorings allow us to observe the variability in transport on short timescales which has been shown to be important both in the RAPID project as a whole and now here for AABW. The ranges in transport estimated are large (2 Sv) and on the order of the range estimated from hydrographic sections. However, mooring data is spatially sparse and in this instance resulted in an estimate of AABW as the net northward transport below 4100 dbar and between 70.5 and 49°W. Hydrographic data allow a more natural estimate of AABW delineated by density or temperature (used here). In comparing the two estimates (below 4100 dbar) and colder than 1.8°C from hydrography, we see that our estimate of transport below 4100 dbar contracts the variability observed when using the full temperature data. (Table 1, column 1 shows a transport range of 2.2–3.7 Sv versus Figure 9b which gives a range of 1.9–4 Sv.) This would suggest that our mooring estimate of AABW transport is actually an underestimate of the true variability.

[31] On comparing properties of AABW, the hydrographic data are superior. The short term variability in temperature from moorings is responsible for the fluctuations observed in transport, but it is difficult to conclude anything from the warming trend observed near the bottom at the MAR moorings. Without further information, the warming signal could be due to a movement in the isotherms delineating AABW or a change in the bulk properties of AABW. In contrast, the warming signal from hydrographic sections is robust and shows that indeed, the deepest, coldest classes of AABW have been warming since 1981 though the volume of water colder than 1.8°C has increased.

[32] The warming observed both globally and in these observations may be due to a change in the source waters of AABW or in advection and mixing along the path from the source regions to 24.5°N. Near the source, recent results have suggested that the export of AABW from the Weddell Sea has been changing: the coldest waters are no longer being exported, possibly due to a localized bottom Ekman effect [*Jullion et al.*, 2010; *Meredith et al.*, 2011]. Understanding changes along the path from the Southern Ocean is more difficult. If transport speeds were to slow, then the observed warming at more northerly latitudes may have resulted from the longer advective timescales which would allow for more mixing with warmer NADW along the pathway. Clearly, rates of transport are better identified using moorings, in order to capture the time variability of the process, but the short term variability observed by the 6 month mooring deployment may not be long enough to infer changes due to processes along the pathway from the Southern Ocean.

[33] One of the motivations for calculating AABW transport variability was to understand its impact on estimates of the MOC at 26°N in the RAPID array. The current RAPID calculation assumes a near steady 2 Sv of northward flowing AABW, peaking at 5500 dbar [*Kanzow et al.*, 2010]. On the basis of the estimates here, the true value may range from 1 to 5 Sv. If the nominal 2 Sv transport currently used in the RAPID estimate of the MOC overturning were reduced to 1 Sv, the estimate of MOC overturning would increase by 0.2 Sv, transferring about 20% of the variability. If the AABW transport were increased to 5 Sv, the MOC overturning estimate would reduce by 0.6 Sv.

While a 0.8 Sv range is within the error estimates for the MOC calculation, it is of the same order as other uncertainties now being quantified.

[34] The balance between the upper and lower MOC cells has been explored in modeling and paleo studies, which suggest a seesaw pattern of dominance shifting between northern hemisphere deep water sources (upper cell) and AABW (lower cell). However, global models are poorly constrained in the deep ocean due to a lack of observations [Saunders *et al.*, 2008]. Besides allowing a direct estimate of deep transport at 24.5°N, these deep moorings will provide temperatures, salinities, and currents which can be used to improve models in their deepest layers.

[35] **Acknowledgments.** The RAPID-WATCH MOC monitoring project is funded by the Natural Environment Research Council (NERC). Data are freely available from <http://www.noc.soton.ac.uk/rapidmoc>. The MOCHA project is funded by the National Science Foundation (NSF) and National Oceanic and Atmospheric Administration (NOAA). The authors would like to thank W. Johns, S. Elipot, J. J.-M. Hirschi, and L. Juillon for helpful discussions. Special thanks to the captain, crew, and science parties involved in the hydrographic section and RAPID/MOCHA mooring deployment and recovery.

References

- Bryden, H. L., H. R. Longworth, and S. A. Cunningham (2005), Slowing of the Atlantic meridional overturning circulation at 25°N, *Nature*, **438**, 655–657.
- Bryden, H. L., A. Mujahid, S. A. Cunningham, and T. Kanzow (2009), Adjustment of the basin-scale circulation at 26°N to variations in Gulf Stream, deep western boundary current and Ekman transports as observed by the RAPID array, *Ocean Sci.*, **5**, 421–433.
- Cunningham, S. A., et al. (2007), Temporal variability of the Atlantic meridional overturning circulation at 26.5°N, *Science*, **317**, 935–938.
- Emery, W. J., and R. E. Thompson (2004), *Data Analysis Methods in Physical Oceanography*, 2nd ed., Elsevier, San Diego, Calif.
- Johns, W. E., L. M. Beal, M. O. Baringer, J. R. Molina, S. A. Cunningham, T. Kanzow, and D. Rayner (2008), Variability of shallow and deep western boundary currents off the Bahamas during 2004–05: Results from the 26°N RAPID–MOC array, *J. Phys. Oceanogr.*, **38**, 605–623.
- Johnson, G. C., and S. C. Doney (2006), Recent western South Atlantic bottom water warming, *Geophys. Res. Lett.*, **33**, L14614, doi:10.1029/2006GL026769.
- Johnson, G. C., S. G. Purkey, and J. M. Toole (2008), Reduced Antarctic meridional overturning circulation reaches the North Atlantic Ocean, *Geophys. Res. Lett.*, **35**, L22601, doi:10.1029/2008GL035619.
- Jullion, L., S. C. Jones, A. C. Naveira Garabato, and M. P. Meredith (2010), Wind-controlled export of Antarctic Bottom Water from the Weddell Sea, *Geophys. Res. Lett.*, **37**, L09609, doi:10.1029/2010GL042822.
- Kanzow, T., et al. (2010), Seasonal variability of the Atlantic meridional overturning circulation at 26.5°N, *J. Clim.*, **23**, 5678–5698.
- King, B. A. (2011), RRS Discovery Cruise 346, Jan–Feb 2010: A transatlantic hydrography section at 24.5°N, *Cruise Rep.*, Natl. Oceanogr. Cent., Southampton, U. K.
- Lavin, A. M., H. L. Bryden, and G. Parrilla (1998), Meridional transport and heat flux variations in the subtropical North Atlantic, *Global Atmos. Ocean Syst.*, **6**, 269–293.
- Lavin, A. M., H. L. Bryden, and G. Parrilla (2003), Mechanisms of heat, freshwater, oxygen and nutrient transports and budgets at 24.5°N in the subtropical North Atlantic, *Deep Sea Res., Part I*, **50**, 1099–1128.
- Limeburner, R., J. A. Whitehead, and C. Cenedese (2005), Variability of Antarctic Bottom Water flow into the North Atlantic, *Deep Sea Res., Part II*, **52**, 495–512.
- Meredith, M. P., A. L. Gordon, A. C. Naveira Garabato, E. P. Abrahamson, B. A. Huber, L. Jullion, and H. J. Venebles (2011), Synchronous intensification and warming of the Antarctic Bottom Water outflow from the Weddell Gyre, *Geophys. Res. Lett.*, **38**, L03603, doi:10.1029/2010GL046265.
- Orsi, A. H., G. C. Johnson, and J. L. Bullister (1999), Circulation, mixing, and production of Antarctic Bottom Water, *Progr. Oceanogr.*, **43**, 55–109.
- Purkey, S. G., and G. C. Johnson (2010), Warming of global abyssal and deep Southern Ocean waters between the 1990s and 2000s: Contributions to global heat and sea level rise budgets, *J. Clim.*, **23**, 6336–6351.
- Rayner, D., et al. (2011), Monitoring the Atlantic meridional overturning circulation, *Deep Sea Res., Part II*, **58**, 1744–1753.
- Saunders, P. M., S. A. Cunningham, B. A. de Cuevas, and A. C. Coward (2008), Decadal changes in the North Atlantic and Pacific meridional overturning circulation and heat flux, *J. Phys. Oceanogr.*, **38**, 2104–2107.
- Trenberth, K. E., and J. M. Caron (2001), Estimates of meridional atmosphere and ocean heat transports, *J. Clim.*, **14**, 3433–3443.
- U. S. Department of Commerce (2006), *Two-minute gridded global relief data*, ETOPO2v2, Boulder, Colo.
- Zenk, W., and E. Morozov (2007), Decadal warming of the coldest Antarctic Bottom Water flow through the Vema Channel, *Geophys. Res. Lett.*, **34**, L14607, doi:10.1029/2007GL030340.

H. Bryden, S. A. Cunningham, E. Frajka-Williams, and B. A. King, National Oceanography Centre, University of Southampton Waterfront Campus, European Way, Southampton, SO14 3ZH, UK. (h.bryden@noc.soton.ac.uk; scu@noc.ac.uk; e.frajka-williams@noc.soton.ac.uk; bak@noc.ac.uk)